

Optimization of Advanced ACTPol Transition Edge Sensor Bolometer Operation Using $R(T,I)$ Transition Measurements

Maria Salatino, Christine G. Pappas, Shawn W. H. Henderson, Laura Newburgh, Michael D. Niemack, Suzanne T. Staggs, and Kasey Wagoner

Abstract—In the current submm and mm cosmology experiments the focal planes are populated by kilopixel transition edge sensors (TESes). Varying incoming power load requires frequent rebiasing of the TESes through standard current–voltage (IV) acquisition. The time required to perform IVs on such large arrays and the resulting transient heating of the bath reduces the sky observation time. We explore a bias step method that significantly reduces the time required for the rebiasing process. This exploits the detectors’ responses to the injection of a small square wave signal on top of the dc bias current and knowledge of the shape of the detector transition $R(T,I)$. This method has been tested on two detector arrays of the Atacama Cosmology Telescope (ACT). In this paper, we focus on the first step of the method, the estimate of the TES $\%R_n$.

Index Terms—Biasing, IV curve, superconducting transition, transition edge sensor (TES).

I. INTRODUCTION

THERE is a rich amount of cosmology and astrophysics to be obtained from measurements in sub-mm and mm bands with angular resolution running from a few arcminutes up to a few degrees.

One particularly exciting example is the primordial B modes, a tiny polarized signal in the Cosmic Microwave Background (CMB) predicted by inflationary theories [1]–[3]. Because the primordial B-mode signal has been constrained to be so small ($<0.1 \mu\text{K}$ on one degree angular scales), we are now at a turning

point where multi-frequency, large surveys of the sky (covering 30-50% of the sky) are necessary to improve our knowledge of the so-called CMB *foregrounds* [4], astrophysical sources such as interstellar dust [5]–[8] and the synchrotron emission [9], whose polarization signals have a B-mode component.

The observations of the CMB foregrounds will also improve the astrophysical knowledge of such sources, for example the dust alignment mechanism with respect to the Galactic magnetic field, the population properties of the interstellar dust grains, and the surrounding environment of accelerated electrons that emit synchrotron radiation. Interactions between the CMB photons and intervening matter (such as gravitational lensing, which converts E modes into B modes [10]) alter the intrinsic CMB signal on arc minute angular scales. Measurements of these effects provide information about the physics of galaxy clusters, structure formation, and neutrino properties (i.e. mass and hierarchy [11]) [12].

The current state-of-the-art detectors used to measure the CMB are already photon-noise limited [13]. In order to improve the signal-to-noise ratio of the CMB measurements discussed above, it is therefore necessary to increase the optical throughput. It can be increased, for example, increasing the focal plane size, decreasing the $F/\#$ or using multi-mode detectors. Here we focus on the first option. Expanding measurements to more frequency bands, as required for separating the primordial B-mode CMB signal from foregrounds, will also require more detectors.

TES bolometers are photon-noise limited detectors used widely in CMB experiments. The straightforward multiplexability of TES bolometers has allowed the development of kilopixel focal plane arrays [14], [15]. Current CMB experiments, both ground-based and balloon-borne, have performed sky observations with such kilo-pixel focal planes. Experiments using focal planes containing anywhere from 3,000 to 10,000 TESes represent the so-called CMB Stage-III: experiments like Advanced ACTPol [16], POLARBEAR2 [17], SPT-3G [18] and Simons Array [19], observe (or will observe) the sky with 5612, 7588, 15234 and 22764 TESes, respectively. The CMB Stage-IV experiment, CMB-S4, will observe the sky with approximately 500k detectors. As we will discuss below, given the wide use of TESes and the increasing size of the focal planes, the efficient *rebiasing* of TES arrays is a key step in the optimal operation of bolometric cameras.

Manuscript received September 7, 2016; accepted January 27, 2017. Date of publication March 1, 2017; date of current version April 3, 2017. This work was supported by the U.S. National Science Foundation through award 1440226. The development of multichroic detectors and lenses was supported by NASA under Grant NNX13AE56G and Grant NNX14AB58G.

M. Salatino, S. T. Staggs, and K. Wagoner are with the Physics Department, Princeton University, Princeton, NJ 08540 USA (e-mail: salatino@princeton.edu; staggs@princeton.edu; kasey.reid.wagoner@gmail.com).

C. G. Pappas was with Princeton University, Princeton 08540, NJ USA. She is now with the National Institute of Standard and Technology (NIST), Boulder, CO 80305 USA (e-mail: christine.pappas@nist.gov).

S. W. Henderson and M. D. Niemack are with Cornell University, Ithaca, NY 14850 USA (e-mail: swh76@cornell.edu; niemack@cornell.edu).

L. Newburgh is with the Dunlap Institute for Astronomy and Astrophysics, University of Toronto, Toronto, ON M5S 3H4, Canada (e-mail: newburgh@di.toronto.ca).

Color versions of one or more of the figures in this paper are available online at <http://ieeexplore.ieee.org>.

Digital Object Identifier 10.1109/TASC.2017.2672687

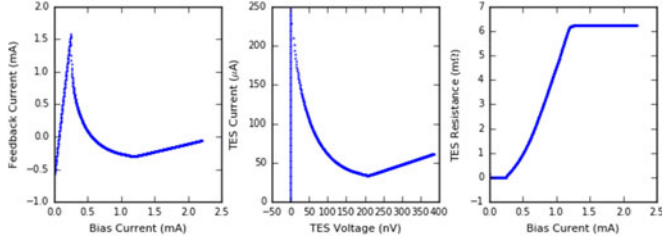


Fig. 2. A typical IV curve from a detector in the ACTPol PA2 array. Left: IV curve in raw units of SQUID feedback current vs. bias current. The SQUID feedback current offset is calculated by fitting a line to the normal branch of this curve. Then, the two plots shown to the right can be trivially generated with knowledge of the bias circuit. Middle: IV curve in units of TES current vs. TES voltage. Right: IV curve converted to units of TES resistance vs. bias current for rebiasing.

offset current is calculated by fitting a line to this part of the IV curve. It is then straightforward to calculate the TES resistance at each I_{bias} value (Fig. 2). Using these R vs. I_{bias} curves for each detector on a bias line, the optimal I_{bias} that biases the most TESes onto their transition is chosen.

Because we can only measure changes in TES current with the SQUIDS, we cannot directly measure the TES resistance at one I_{bias} value. One way to calculate the overall current offset and then the TES resistance is to take an IV curve, as described above. Under certain conditions, using a previously measured template, it is also possible to calculate the TES resistance at one I_{bias} value with only a bias step measurement around that I_{bias} point.

During the bias step measurement, we perturb I_{bias} slightly and measure the local slope dI/dI_{bias} . The relationship between the bias step slope and the TES resistance is given by [25]:

$$R = r_{sh} \left(1 - \left(\frac{\Delta I}{\Delta I_{bias}} \right)^{-1} \right) \frac{L - 1}{1 + \beta + L}, \quad (1)$$

where I is the TES current, L is the loop gain defined by Irwin and Hilton [15]:

$$L = \frac{P_{bias} \alpha}{GT}. \quad (2)$$

P_{bias} is the electrical power due to the voltage bias on the TES, α (β) is the local logarithmic derivative of the TES resistance versus TES temperature (current), and G is the thermal conductivity between the TES island and the bath.

Instead of calculating the above function from TES properties measured under all relevant conditions, we can equivalently directly calculate the two-dimensional function $R(dI/dI_{bias}, I_{bias})$ from a set of IV curves. We can then use this template to calculate the TES resistance from a bias step measurement.

The shape of the TES superconducting transition ($R(T,I)$) is implicitly included in this template, as equation (1) depends on α and β . TES bolometers are usually operated with strong electrothermal feedback and have high loop gain. In the limit of infinite loop gain, equation (1) reduces to:

$$R = r_{sh} \left(1 - \left(\frac{\Delta I}{\Delta I_{bias}} \right)^{-1} \right), \quad (3)$$

which does not depend on any detector properties.

We find that for the ACTPol and AdvACT detectors, accurate calculation of the resistance from a bias step requires the use of the full expression (1), especially when the $R(T,I)$ transitions have non-linearities.

It is important to note that for particularly poorly behaved detectors, the map from $(dI/dI_{bias}, I_{bias})$ to R may not be well-defined: there may be multiple values of R in the template that a given $(dI/dI_{bias}, I_{bias})$ pair could map to. In this case, the detector resistance could be determined by taking bias steps often enough (with respect to the rate of atmosphere loading drift) that the choice between the multiple resistance values given by the template is obvious based on the previously measured resistance value.

After measuring each TES's resistance with a bias step, the new optimal I_{bias} value could be determined without taking an IV curve in one of two ways. The first method would consist of repeatedly adjusting I_{bias} (either decreasing if the TES resistance are too high or increasing if the TES resistances are too low) and measuring the new TES resistances until a suitable I_{bias} value is found.

The second method exploits the fact that a detector's IV curve only depends on the $P_{loading}$ value [22], where $P_{loading}$ is defined by:

$$P_{loading} = \eta P_{\gamma} + kT_b^n = kT^n - P_{bias}.$$

If the map from $(I_{bias}, dI/dI_{bias})$ to $P_{loading}$ is uniquely defined, one can find the previously measured IV curve with a dI/dI_{bias} slope at I_{bias} closest to the measured value from the bias step, then use this IV curve to re-bias the detectors as usual.

In this proceedings, we discuss the results of a procedure for the first step of both of these rebiasing processes: calculating the TES resistance from the bias step measurement.

A. The TES Response to a Bias Steps Signal

A small amplitude ($dI_{bias} = 10\mu\text{A}$ wide (50 DAC); period = 1 second) square wave voltage signal is injected on top of the DC bias current (of order 1-2 mA) I_{bias} applied to the TES. For each bias step 2000 samples are acquired, resulting in 10 square wave periods. A suitable algorithm locates the TES feedback current step, dI_{fb} , produced in response to the bias step signal by finding the data indices where the difference between consecutive current values exceeds the median value more than 5 standard deviations. Since TESes are read out with SQUIDS, we measure the current of the feedback coil of the TES readout circuit. The knowledge of the readout circuit is then used to estimate dI .

B. The Template Spanning the TES Operational Parameters

To calculate the TES $\%R_n$ from a bias step, we first generate a unique template for each detector that maps $(I_{bias}, dI/dI_{bias})$ to $\%R_n$ using IVs taken during previous seasons of observations. For each IV curve, we calculate dI/dI_{bias} and $\%R_n$ for each I_{bias} point and add these data points to the template. From the analysis of many IVs taken under different optical loading conditions and bath temperatures, we reconstruct

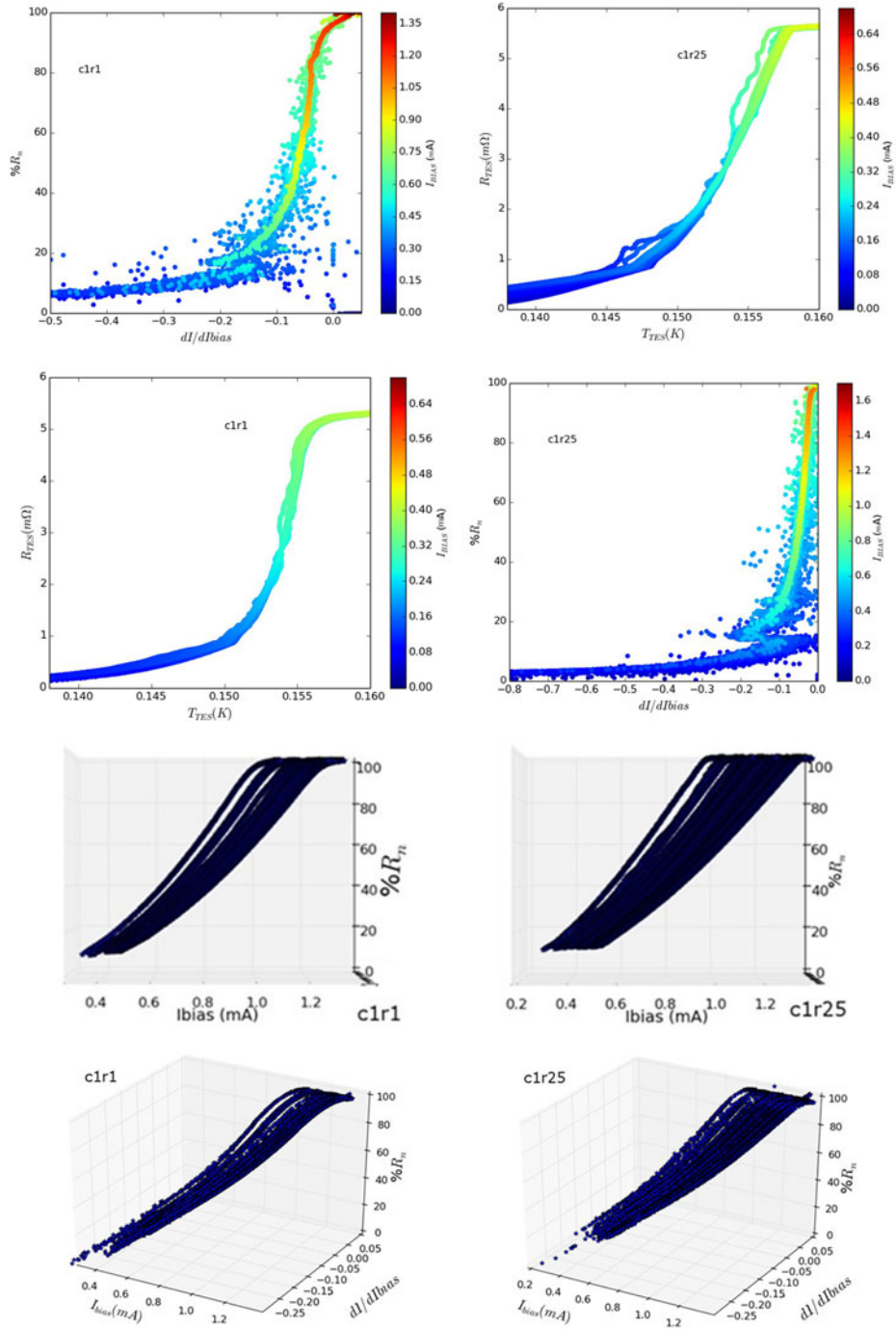


Fig. 3. ACTPol PA3, top: $\%R_n(dI/dI_{bias})$, TES normal resistance versus TES response to a bias steps signal. At low $\%R_n$, the TES response results in a noisy behavior. Center: $R_{TES}(T_{TES})$ to study the shape of the TES superconducting transition; the width of the transition is generally small (i.e. few mK) with a less flat trend at lower temperatures. Bottom: the template $\%R_n(I_{bias}, dI/dI_{bias})$ used to estimate the optimal bias current, each template is built from a set of 100 IVs. We also report the plot $\%R_n(I_{bias})$ from the template. For each ACTPol PA3 TES we built the template, here we report the plots for two TESes: c1r1 and c1r25.

the parameter space spanned during typical operation. Typical templates built from on the order of 100 IVs are shown in Figs. 3 and 4.

The bias step measurement provides a pair of values (I_{bias} , dI/dI_{bias}) for each TES fed by a given I_{bias} . This point (I_{bias} , dI/dI_{bias}) is interpolated inside the template (I_{bias} , dI/dI_{bias} , $\%R_n$) to estimate the $\%R_n$, since the interpolation method was

found to give a better estimate of the $\%R_n$ value than fitting with an analytical expression. The algorithm estimates the $\%R_n$ from the TES response to a bias steps signal by comparing the results of three different interpolation algorithms (closest, linear and cubic). Below we describe how this method has been implemented for testing the PA3 ACTPol and the AdvACT HF TESes.

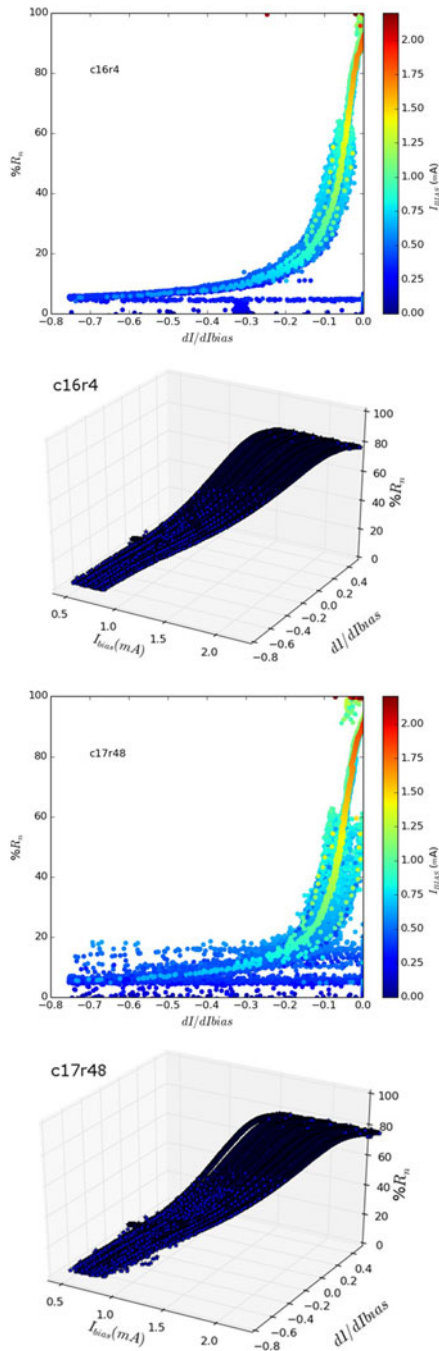


Fig. 4. AdvACT HF NW, top: $\%R_n(dI/dI_{bias})$, TES normal resistance versus TES response to a bias steps signal. At low $\%R_n$, the TES response results in a noisy behavior. Bottom: the template $\%R_n(I_{bias}, dI/dI_{bias})$ used to estimate the optimal bias current, each template is built from a set of 100 IVs. For each AdvACT HF NW TES we built the template, here we report the plots for two TESes: c16r4 and c17r48.

III. TESTS ON ACT TESSES

The ACTpol PA3 array is composed of about 1000 TESes fed by 29 bias lines. Typically on ACT, IVs are acquired every 2-3 hours, while bias steps are acquired on time scales shorter than 30 minutes. Initially we built templates from all the IVs collected

from an entire past observing season, then we restricted the analysis on a subset of IVs. In Fig. 3 we report the typical trend of $\%R_n(dI/dI_{bias})$ and the template we built from 100 IVs acquired during the past ACT observation season. We also plot the TES $R(T)$ transitions that show a behavior close to the ideal one or small deviations from it (Fig. 3).

AdvACT HF is divided in four sectors (NW, NE, SW and SE), each of which is fed by six bias lines. In this first work we present the tests performed on the NW sector. The $\%R_n(dI/dI_{bias})$ and the templates from typical AdvACT detectors are reported in Fig. 4.

The overall target is to improve TES operation by reducing the time to set the optimal bias current with respect to the standard IV analysis. The total time comes from three times: measurement time (IV or bias steps), dead time due to heating (since we need to wait the cool down back to the working temperature) and the analysis time (the IV, or the bias step, is analyzed to estimate the optimal bias current). For the standard IV method: the running time takes 1-2 minutes, the dead time few minutes and the analysis time less than one minute. For the bias steps method: the running time takes few seconds, the dead time is null since the bias step (given the involved current, about 10 μ A, with respect to IV, up to 1.5mA) does not heat up the focal plane and the analysis time (currently) is about 1 minute. We want to reduce the analysis time: if, with the bias steps method, we already saved time for the first two steps but the third step ends to be more time consuming than the traditional method, the advantages in using the bias steps method become less strong and we could end setting the optimal TES bias voltage with a similar amount of time.

Instead of building the template for all the IVs acquired during an entire season, the template is built with order of 100 IVs. This avoids spreading the interpolation resolution over the entire template and reduces the time necessary to run the analysis since the most time consuming operation in this method is the template interpolation. To reduce the time, the algorithm doesn't perform the interpolation on the entire template but only on a subset. It starts interpolating a subset of data that deviates less than 1% from the pair of values $(I_{bias}, dI/dI_{bias})$. If no interpolated point is found, the script is run again increasing the deviation threshold, in steps of 5%, from 5% to 85%, until the interpolated point is found. If no point is found, the script performs the interpolation on the entire template.

The typical time for running the interpolation on a subset of the template on order of 800 TESes is 50 s on a Intel Core i5-4670 (3.40GHz) computer with 8 Gb of memory.

For the ACTPol PA3 array, we have compared the $\%R_n$ calculated with our bias step method to the $\%R_n$ calculated from the IV acquired most recently before the bias step (typically 5 minutes before). When a bias steps measurement is acquired a short time after the previous IV the agreement between the $\%R_n$ estimated with the two methods is good (Fig. 5), the distribution of the error has a typical 75th percentile of about $3\%R_n$. In the case of bias steps acquired after a significant amount of time, the fluctuations of the weather conditions reduce the agreement.

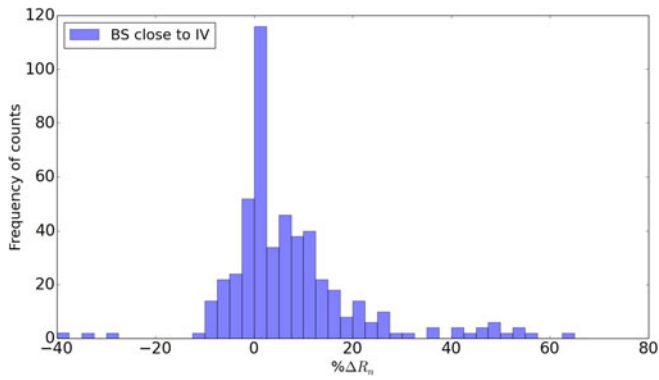


Fig. 5. Histogram of the error of the estimated TES $\%R_n$ from the standard IV analysis and the bias steps analysis. The analysis refers to ACTPol PA3 detectors and a bias steps measurement taken few minutes after the corresponding IV. Few outliers detectors have been removed from the histogram.

The study of the evolution of the percentile of the distribution can be used to forecast the necessity of acquire another IV.

IV. CONCLUSION

We explored a new method, first presented in [22], for estimating the optimal bias current that should be applied to the TESes (rebiasing process) which exploits the knowledge of the TES $R(T,I)$ transitions and the injection of a small square wave signal on the DC bias current. In this work we focused on the first part of the method: the estimate of the TES resistance with bias steps measurements. The second part, the estimate of the optimal current bias, will be the subject of a following future publication. This method, tested on the PA3 ACTPol and HF AdvACT TESes, avoids the transient bath heating produced by the standard IV analysis and significantly reduces the time required for the rebiasing process.

REFERENCES

- [1] D. Baumann *et al.*, "Probing inflation with CMB polarization," *AIP Conf. Proc.*, vol. 1141, pp. 10–120, 2009.
- [2] K. N. Abazajian, K. Arnold, and J. Austermann, "Inflation physics from the cosmic microwave background and large scale structure," *Astroparticle Phys.*, vol. 63, pp. 55–65, 2015.
- [3] A. D. Linde, "Particle physics and inflationary cosmology," *Contemp. Concepts Phys.*, vol. 5, pp. 1–362, 1990.
- [4] M. Tucci, E. Martínez-González, P. Vielva, and J. Delabrouille, "Limits on the detectability of the CMB B-mode polarization imposed by foregrounds," *Monthly Notices Roy. Astron. Soc.*, vol. 360, no. 3, pp. 935–949, 2005.
- [5] S. Prunet and A. Lazarian, "Polarized foreground from thermal dust emission," *Rev. for the Workshop: Sloan Summit on Microwave Backgrounds*, A. De Oliveira-Costa and M. Tegmark, Eds. eprint arXiv:astro-ph/9902314, p. 345, 1999.
- [6] J. E. Vaillancourt, "Polarized emission from interstellar dust," *EAS Publ. Ser.*, vol. 23, pp. 147–164, 2007.
- [7] BICEP2 and Planck Collaboration, "Joint analysis of BICEP2/Keck Array and Planck data," *Phys. Rev. Lett.*, vol. 114, no. 10, 2015, Art. no. 101301.
- [8] Planck Collaboration, "Planck intermediate results. XIX. An overview of the polarized thermal emission from galactic dust," *Astronomy & Astrophys.*, vol. 576, 2015, Art. no. A104.
- [9] Planck Collaboration, "Planck 2015 results. XXV. Diffuse low-frequency galactic foregrounds," *Astronomy & Astrophys.*, vol. 594, p. A25, astro-ph/1506.06660, 2016.
- [10] A. Lewis and A. Challinor, "Weak gravitational lensing of the CMB," *Phys. Rep.*, vol. 429, pp. 1–65, 2006.
- [11] R. Allison, P. Caucal, E. Calabrese, J. Dunkley, and T. Louis, "Towards a cosmological neutrino mass detection," *Phys. Rev. D*, vol. 92, no. 12, 2015, Art. no. 123535.
- [12] K. N. Abazajian *et al.*, "Neutrino physics from the cosmic microwave background and large scale structure," *Astroparticle Phys.*, vol. 63, pp. 66–80, 2015.
- [13] BICEP2 Collaboration, Keck Array Collaboration, and SPIDER Collaboration, "Antenna-coupled TES bolometers used in BICEP2, Keck Array, and Spider," *Astrophysical J.*, vol. 812, no. 2, 2015, Art. no. 176.
- [14] K. D. Irwin, "SQUID multiplexers for transition-edge sensors," *Phys. C: Supercond.*, vol. 368, no. 1–4, pp. 203–210, 2002.
- [15] K. D. Irwin and G. C. Hilton, "Transition-edge sensors," *Cryogenic Particle Detection (Topics in Applied Physics 99)*. Berlin, Germany: Springer, 2005, pp. 63–150.
- [16] S. W. Henderson *et al.*, "Advanced ACTPol cryogenic detector arrays and readout," *J. Low Temp. Phys.*, vol. 184, no. 3–4, pp. 772–779, 2016.
- [17] A. Suzuki *et al.*, "The Polarbear-2 and the Simons Array Experiments," *J. Low Temp. Phys.*, vol. 184, no. 3–4, pp. 805–810, 2016.
- [18] B. A. Benson, P. A. R. Ade, and Z. Ahmed, "SPT-3G: A next-generation cosmic microwave background polarization experiment on the South Pole telescope," *Proc. SPIE*, vol. 9153, 2014, Art. no. 91531P.
- [19] K. Arnold *et al.*, "The Simons array: Expanding POLARBEAR to three multi-chroic telescopes," *Proc. SPIE*, vol. 9153, 2014, Art. no. 91531F.
- [20] S. W. Henderson, J. R. Stevens, M. Amiri *et al.*, "Readout of two-kilopixel transition-edge sensor arrays for Advanced ACTPol," *Proceedings of the SPIE*, vol. 9914, p. 99141G, astro-ph/1607.06064, 2016.
- [21] D. Prêle *et al.*, "A 128 multiplexing factor time-domain squid multiplexer," *J. Low Temp. Phys.*, vol. 184, pp. 363–368, 2016.
- [22] C. G. Pappas, "Assembly, characterization, and operation of large-scale TES detector arrays for ACTPol," Ph.D. dissertation, Phys. Dept., Princeton Univ., Princeton, NJ, USA, 2016.
- [23] R. J. Thornton *et al.*, "The Atacama Cosmology Telescope: The polarization-sensitive ACTPol instrument," *The ApJ Supp. Ser.*, vol. 227, no. 2, id. 21, astro-ph/1605.06569, 2016.
- [24] S. P. Ho *et al.*, "The first multichroic polarimeter array on the Atacama cosmology telescope: Characterization and performance," *J. Low Temp. Phys.*, vol. 184, no. 3, pp. 559–567, 2016.
- [25] L. Dale *et al.*, "AlMn transition edge sensors for Advanced ACTPol," *J. Low Temp. Phys.*, vol. 184, no. 1, pp. 66–73, 2016.
- [26] W. B. Doriese *et al.*, "Developments in time-division multiplexing of X-ray Transition-Edge Sensors," *J. Low Temp. Phys.*, vol. 184, no. 1–2, pp. 389–395, 2016.